

# Instanton effects on charmonium states

Ulugbek Yakhshiev,<sup>1,\*</sup> Hyun-Chul Kim,<sup>1,2,3,†</sup> and Emiko Hiyama<sup>2,4,5,‡</sup>

<sup>1</sup>*Department of Physics, Inha University, Incheon 22212, Republic of Korea*

<sup>2</sup>*Advanced Science Research Center, Japan Atomic Energy Agency, Shirakata, Tokai, Ibaraki, 319-1195, Japan*

<sup>3</sup>*School of Physics, Korea Institute for Advanced Study (KIAS), Seoul 02455, Republic of Korea*

<sup>4</sup>*Department of Physics, Kyushu University, 819-0395, Fukuoka, Japan*

<sup>5</sup>*RIKEN Nishina Center, RIKEN, 2-1 Hirosawa, 351-0115 Saitama, Japan*

(Dated: March 17, 2022)

The instanton effects on the charmonium spectrum is discussed in the framework of nonrelativistic potential model. The results from constituent quark model without inclusion of instanton effects is compared with the results for ‘the potential from constituent quark model + the contribution from the instanton liquid model’. We consider two models with the corresponding instanton potentials and discuss their relevance to explanations of the origin phenomenological parameters used in the nonrelativistic potential models. We also present the universal instanton potential in the parametrized form which can be useful in practical calculations.

PACS numbers: 12.38.Lg, 12.39.Pn, 14.40.Pq

Keywords: Instanton-induced interactions, heavy-quark potential, quarkonia.

## I. INTRODUCTION

Physics of charmonia has entered a new era, since the finding of the first narrow exotic charmonium was reported by the Belle Collaboration [1]. Many narrow exotic charmonium states have been consecutively observed [2–13] and were coined collectively the XYZ mesons (see recent reviews [14, 15]). These new exotic charmonium states have drawn considerable attention (see for example the reviews in Refs. [16–21]) and also brought about multifaceted view point on conventional charmonium states.

Theoretically, the quantum-mechanical potential models provide an easy but very effective way of describing the charmonum spectrum [17–19, 22, 23]. In a standard approach there are basically two main contributions to the heavy-quark potential for the charmonium system: the Coulomb-like potential and the phenomenological quark-confining one. The Coulomb-like potential originates from one-gluon exchange (OGE) between a heavy quark ( $Q$ ) and a heavy anti-quark ( $\bar{Q}$ ) [24–27], based on perturbative quantum chromodynamics (pQCD). Note that the static Coulomb-like potential was scrutinized already to higher-order corrections from pQCD [28–32]. By nature of pQCD, the Coulomb-like interactions are supposed to govern the short-range physics of the charmonia. At large distances the strength of the Coulomb-like interaction decreases. However, the presence of the quark-confining potential makes the strength of the total interaction increase. This is due to the fact that any quark inside a charmonium is ordained to be confined in it, effects of the quark confinement [33] are necessarily involved. The heavy-quark potential for the quark

confinement can be obtained at least phenomenologically from the Wilson loop, which rises linearly at large distances [22, 23]. On the other hand, as the quark and the anti-quark start to recede from each other the certain nonperturbative contributions come into play.

Recently, we examined yet another nonperturbative effects on the mass spectrum of the charmonia from the instanton vacuum of QCD [34]. The central part of the heavy-quark potential was already derived by Diakonov et al. [35], based on the instanton liquid model for the QCD vacuum [36–38]. The spin-dependent part of the instanton-induced potential can be easily obtained by employing the method of Eichten and Feinberg [39]. There are two intrinsic parameters of characterizing the instanton vacuum, i.e. the average size of the instanton  $\rho$  and the average distance  $R$  between instantons. Their numerical values were estimated to be  $\rho \approx 0.33$  fm and  $R \approx 1$  fm [36, 37, 40]. However, these values are just the approximated ones. For example, Refs. [41–43] considered  $1/N_c$  meson-loop contributions in the light-quark sector and found it necessarily to readjust the values of parameters as  $\rho \simeq 0.35$  fm and  $R \simeq 0.86$  fm. In Ref. [34], we scrutinized the dependence of the heavy-quark potential from the instanton vacuum. In the present work, we combine the instanton-induced heavy-quark potential with the Coulomb-like and quark-confinement potentials and investigate explicitly the instanton effects on the mass spectrum of the charmonia.

The paper is organized as follows: In Section II, we explain briefly the nonrelativistic heavy-quark potential model consisting of the color Coulomb-like potential and the linear scalar potential for quark confinement [44] and discuss the contribution to the total heavy-quark potential from the instanton vacuum. In Section III, the Gaussian expansion method for a numerical calculation will shortly be described. In Section IV we present the results and discuss them. The final Section V is devoted to the summary and conclusions of this work.

\* yakhshiev@inha.ac.kr

† hchkim@inha.ac.kr

‡ hiyama@phys.kyushu-u.ac.jp

## II. HEAVY-QUARK POTENTIAL

The standard heavy-quark potential consists of the four different terms, written as

$$\begin{aligned} V_{Q\bar{Q}}(\mathbf{r}) = & V_C(r) + V_{SS}(r)(\mathbf{S}_Q \cdot \mathbf{S}_{\bar{Q}}) \\ & + V_{LS}(r)(\mathbf{L} \cdot \mathbf{S}) \\ & + V_T(r) [3(\mathbf{S}_Q \cdot \mathbf{n})(\mathbf{S}_{\bar{Q}} \cdot \mathbf{n}) - \mathbf{S}_Q \cdot \mathbf{S}_{\bar{Q}}], \end{aligned} \quad (1)$$

where  $V_C$ ,  $V_{SS}$ ,  $V_{LS}$  and  $V_T$  represent respectively the central, spin-spin, spin-orbit and tensor parts of the heavy-quark potential.  $\mathbf{S}_Q$ ,  $\mathbf{S}_{\bar{Q}}$ , and  $\mathbf{L}$  denote the spin operator of a heavy quark, that of a heavy anti-quark, and the relative orbital angular momentum operator, respectively. The unit vector  $\mathbf{n}$  in three dimensional ordinary space is chosen in direction of the line joining the centers of the heavy quark and heavy anti-quark. All contributions to the total  $Q\bar{Q}$  potential can be constructed within the framework of nonrelativistic potential approaches. As mentioned previously, the color Coulomb-like vector potential arises from OGE between  $Q$  and  $\bar{Q}$  while the linear scalar potential is constructed phenomenologically from the area law of the Wilson loop [33] for the quark confinement. We denote the corresponding *OGE vector + scalar confining potential* as  $V^{(P)}$ . In addition, we introduce the nonperturbative potential  $V^{(NP)}$  derived from the instanton vacuum [34]. Consequently, the heavy-quark potential in the present work is written as

$$V(r) = V^{(P)}(r) + V^{(NP)}(r). \quad (2)$$

We will compute the mass spectrum of the charmonia based on the potential in Eq. (2). However, we want to emphasize that we will not carry out a fine tuning to reproduce the experimental data, since it is of greater importance to understand the nonperturbative effects coming from the instanton-induced potential and physical implications of the parameters involved.

### A. Heavy-quark potential

A nonrelativistic potential model [44] provides a minimal theoretical framework to describe the charmonia. The central part of the heavy-quark potential is expressed as

$$V_C^{(P)}(r) = \kappa r - \frac{4\alpha_s}{3r}, \quad (3)$$

where the first term expresses the linear scalar potential for the quark confinement and the second one comes from OGE, respectively. Here  $\kappa$  stands for the parameter of the string tension, of which the numerical value can be approximately determined by reproducing the mass spectrum of the charmonia. The parameter  $\alpha_s$  denotes the running strong coupling constant of pQCD, of which the value is theoretically well-known. We fix the scale of  $\alpha_s$

at the mass of the charm quark. We will discuss physical implications of these two parameters later.

The spin-dependent parts can be obtained from the central potential (3)

$$V_{SS}^{(P)}(r) = \frac{32\pi\alpha_s}{9m_Q^2} \tilde{\delta}_\sigma(r), \quad (4)$$

$$V_{LS}^{(P)}(r) = \frac{1}{2m_Q^2} \left( \frac{4\alpha_s}{r^3} - \frac{\kappa}{r} \right), \quad (5)$$

$$V_T^{(P)}(r) = \frac{4\alpha_s}{m_Q^2 r^3}, \quad (6)$$

which appear from the next-to-leading order in the expansion of the heavy quark mass  $m_Q$ . So, the spin-dependent potentials are proportional to  $1/m_Q^2$ , respectively. In the present work, the value of the charm-quark mass  $m_c$  will be determined by including the instanton effects. A *smearred* Dirac delta function  $\tilde{\delta}_\sigma$  in Eq. (4) is written in the Gaussian form

$$\tilde{\delta}_\sigma(r) = \left( \frac{\sigma}{\sqrt{\pi}} \right)^3 e^{-\sigma^2 r^2}, \quad (7)$$

where  $\sigma$  is the smearing parameter that can be determined phenomenologically.

### B. Instanton-induced potential

In addition to the potential given in Eq. (3), we introduce the instanton-induced potential, which was already derived in Refs. [34, 35]. The explicit form of the potential is expressed as

$$V_C^{(NP)}(r) = \frac{4\pi\rho^3}{N_c R^4} \mathcal{I}\left(\frac{r}{\rho}\right), \quad (8)$$

where  $N_c$  denotes the number of colors,  $\rho$  and  $R$  stand for the average instanton size and average inter-instanton distance. The dimensionless integral  $\mathcal{I}(x)$  is given as a function of the dimensionless variable  $x$

$$\begin{aligned} \mathcal{I}(x) = & \int_0^\infty y^2 dy \int_{-1}^1 dt \left\{ 1 - \cos\left(\frac{\pi y}{\sqrt{y^2 + 1}}\right) \right. \\ & \times \cos\left(\pi \sqrt{\frac{y^2 + x^2 + 2xyt}{y^2 + x^2 + 2xyt + 1}}\right) \\ & - \frac{y + xt}{\sqrt{y^2 + x^2 + 2xyt}} \sin\left(\frac{\pi y}{\sqrt{y^2 + 1}}\right) \\ & \left. \times \sin\left(\pi \sqrt{\frac{y^2 + x^2 + 2xyt}{y^2 + x^2 + 2xyt + 1}}\right) \right\}. \end{aligned} \quad (9)$$

Though it is possible to compute Eq. (9) numerically given  $x$ , it is more convenient to parametrize the integral  $\mathcal{I}(x)$  such that one can easily make it useful for a

practical calculation. We obtain a suitable parametrization as follows

$$\tilde{\mathcal{I}}(x) = \mathcal{I}_0 \left[ 1 + \sum_{i=1}^3 a_i x^{2(i-1)} e^{-b_i x^2} + \frac{a_4}{x} (1 - e^{-b_4 x^2}) \right], \quad (10)$$

where the prefactor  $\mathcal{I}_0$  is expressed in terms of the Bessel functions

$$\mathcal{I}_0 = -\frac{2\pi^3}{3} \left( J_0(\pi) + \frac{1}{\pi} J_1(\pi) \right) \quad (11)$$

and the parameters  $a_i$ 's and  $b_i$ 's are summarized in the following matrix forms

$$a = \begin{pmatrix} -1 \\ 0.10184 \\ 0.00064 \\ -1.11267 \end{pmatrix}, \quad b = \begin{pmatrix} 0.25135 \\ 0.70255 \\ 0.18625 \\ 0.04644 \end{pmatrix}. \quad (12)$$

One can inspect whether the parametrized function  $\tilde{\mathcal{I}}$  in Eq. (10) yields the correct limiting values of the original integral  $\mathcal{I}(x)$  in Eq. (9) at  $x = 0$  and  $x \rightarrow \infty$ . That is, the following relations

$$\begin{aligned} \lim_{x \rightarrow 0} \mathcal{I}(x) &= \lim_{x \rightarrow 0} \tilde{\mathcal{I}}(x) = 0, \\ \lim_{x \rightarrow \infty} \mathcal{I}(x) &= \lim_{x \rightarrow \infty} \tilde{\mathcal{I}}(x) = \mathcal{I}_0. \end{aligned}$$

are well satisfied. At small  $x \ll 1$ ,  $\mathcal{I}(x)$  can be analytically evaluated as

$$\begin{aligned} \mathcal{I}(x) &\simeq \frac{\pi^2}{3} \left[ \frac{\pi}{16} - J_1(2\pi) \right] x^2 \\ &\quad - \pi \left[ \frac{\pi^2(438 + 7\pi^2)}{30720} + \frac{J_2(2\pi)}{80} \right] x^4 \\ &= 1.34467x^2 - 0.500508x^4, \end{aligned} \quad (13)$$

while the parametrization of Eq. (10) gives the result

$$\begin{aligned} \tilde{\mathcal{I}}(x) &\simeq \mathcal{I}_0(-a_1 b_1 + a_2 + a_4 b_4) x^2 \\ &\quad + \frac{\mathcal{I}_0}{2} (a_1 b_1^2 - 2a_2 b_2 + 2a_3) x^4 \\ &= 1.3316x^2 - 0.452657x^4. \end{aligned} \quad (14)$$

At large  $x$ , the limiting results of  $\mathcal{I}(x)$  and  $\tilde{\mathcal{I}}(x)$  are produced as

$$\mathcal{I}(x) \simeq \mathcal{I}_0 - \frac{\pi^2}{2x} = 4.41625 - \frac{4.9348}{x}, \quad (15)$$

$$\tilde{\mathcal{I}}(x) \simeq \mathcal{I}_0 \left( 1 + \frac{a_4}{x} \right) = 4.41625 - \frac{4.91384}{x}, \quad (16)$$

respectively. From Eqs. (13)–(16), one can see that the corresponding coefficients of the asymptotic forms are very close to each other.

In general, the parametrization in Eq. (10) interpolates the numerical value of the integral  $\mathcal{I}(x)$  with a very good accuracy in the whole range of  $x$ . In Fig. 1, the numerical result of Eq. (9) is compared with that from the parametrization in Eq. (10). As shown in Fig. 1, they overlap completely each other in the whole range of  $x$ . The maximal value of a relative error is located only at

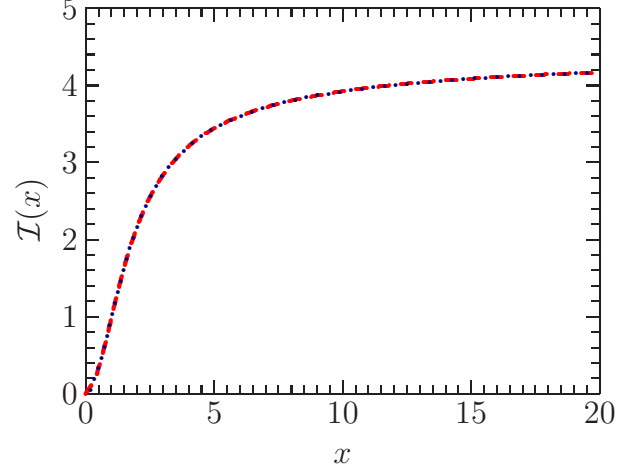


FIG. 1. (Color online) The dimensionless integral  $\mathcal{I}(x)$  from the instanton vacuum. The numerical result of Eq. (9) is depicted as the red dashed curve whereas that of parametrization given in Eq. (10) is drawn as the blue dotted curve.

small  $x$  region and does not exceed the value

$$\begin{aligned} \lim_{x \rightarrow 0} \frac{\mathcal{I}(x) - \tilde{\mathcal{I}}(x)}{\mathcal{I}(x)} &= 1 \\ &\quad - I_0(b_1 + a_2 + a_4 b_4) \left\{ \frac{\pi^2}{3} \left[ \frac{\pi}{16} - J_1(2\pi) \right] \right\}^{-1} \\ &= 0.00972. \end{aligned} \quad (17)$$

At large values of  $x \rightarrow \infty$ , the relative error decreases according to the formula

$$\frac{\mathcal{I}(x) - \tilde{\mathcal{I}}(x)}{\mathcal{I}(x)} \approx -\frac{0.00475}{x - 1.11742}. \quad (18)$$

The spin-dependent parts of the heavy-quark potential from the instanton vacuum can be obtained from the central part according to the following formulas

$$V_{SS}^{(\text{NP})}(r) = \frac{1}{3m_Q^2} \nabla^2 V_C^{(\text{NP})}(r), \quad (19)$$

$$V_{LS}^{(\text{NP})}(r) = \frac{1}{2m_Q^2} \frac{1}{r} \frac{dV_C^{(\text{NP})}(r)}{dr}, \quad (20)$$

$$V_T^{(\text{NP})}(r) = \frac{1}{3m_Q^2} \left( \frac{1}{r} \frac{dV_C^{(\text{NP})}(r)}{dr} - \frac{d^2 V_C^{(\text{NP})}(r)}{dr^2} \right). \quad (21)$$

Using the parametrization we introduced above, we can compute almost all integrations for the instanton-induced

potential analytically. The merit of the parametrization given in Eq. (10) is not limited to the simple calculation of the integration  $\mathcal{I}(x)$ . In fact, the instanton-induced central potential is expressed in terms of  $\mathcal{I}(x)$  with all other instanton parameters factored out. It means that  $\mathcal{I}(x)$  can be used in the universal way for any set of the instanton parameters. So, the spin-dependent potentials in Eqs. (19)–(21) can be also expressed in terms of  $\mathcal{I}(x)$  for any heavy-quark degrees of freedom, i.e. for the charmonia or bottomonia.

The instanton liquid model for the QCD vacuum has two important intrinsic parameters: the average size of the instanton  $\rho$  and the average inter-distance  $R$  between instantons. In fact, the  $Q\bar{Q}$  potential is sensitive to them. Thus, we will consider three different sets of instanton parameters by changing them in a permissible manner. Model I (M-I) uses the original values of the instanton parameters:  $\rho \simeq 0.33$  fm and  $R \simeq 1$  fm. However,  $\rho$  and  $R$  can be changed in a different situation. For example, Refs. [41–43] considered the  $1/N_c$  meson-loop contributions in the light-quark sector and found it necessary to readjust them as  $\rho \simeq 0.35$  fm and  $R \simeq 0.856$  fm. Model IIa (M-IIa) employs these values as in Ref. [34]. In lattice QCD, the instanton vacuum was simulated and the following values were suggested:  $\rho \approx 0.36$  fm and  $R \approx 0.89$  fm [45–48], which are almost the same as those with the  $1/N_c$  meson-loop corrections. Therefore, the model with this set is referred as Model IIb (M-IIb) also as in Ref. [34]. The parameter dependence of the potential can be easily understood from the form of the leading-order potential expressed in Eq. (8). While the prefactor  $\rho^3/R^4 N_c$ , which includes both the parameters, governs the overall strength of the potential, its range is dictated only by the average instanton size  $\rho$  through the dimensionless integral  $\mathcal{I}(r/\rho)$ .

### III. NUMERICAL METHOD

In order to evaluate the bound states in the spectrum of the quarkonia, we have to solve the Schrödinger equation [52]

$$(\hat{H} - E)|\Psi_{JJ_3}\rangle = 0, \quad (22)$$

where  $\hat{H}$  is the Hamiltonian operator and  $|\Psi_{JJ_3}\rangle$  represents the corresponding state vector with the total angular momentum  $J$  and its third component  $J_3$ . The projection of the state vector  $\langle r|\Psi_{JJ_3}\rangle$  will reproduce the representation of the Hamiltonian in coordinate space

$$\hat{H}(\mathbf{r}) = -\frac{\hbar^2}{m_Q}\nabla^2 + V_{Q\bar{Q}}(\mathbf{r}), \quad (23)$$

where  $\mu_Q$  arises from the reduced mass of the quarkonium system. The matrix elements of the  $Q\bar{Q}$  potential in the standard basis  $|^{2S+1}L_J\rangle$ , which is given in terms of the total spin  $S$ , the orbital angular momentum  $L$ , and

the total angular momentum  $J$  satisfying the relation  $\mathbf{J} = \mathbf{L} + \mathbf{S}$ , are obtained as

$$\begin{aligned} V_{Q\bar{Q}}(r) &= \langle^{2S+1}L_J|V_{Q\bar{Q}}(\mathbf{r})|^{2S+1}L_J\rangle \\ &= V(r) + \left[\frac{1}{2}S(S+1) - \frac{3}{4}\right]V_{SS}(r) \\ &\quad + \langle\mathbf{L} \cdot \mathbf{S}\rangle V_{LS}(r) + \langle\mathbf{\Omega}_T\rangle V_T(r). \end{aligned} \quad (24)$$

Here the matrix element of the tensor operator is obtained to be

$$\begin{aligned} \langle\mathbf{\Omega}_T\rangle &= \frac{S(S+1)L(L+1)}{3(2L-1)(2L+3)} \\ &\quad - \frac{2\langle\mathbf{L} \cdot \mathbf{S}\rangle[2\langle\mathbf{L} \cdot \mathbf{S}\rangle + 1]}{4(2L-1)(2L+3)} \end{aligned} \quad (25)$$

and  $\langle\mathbf{L} \cdot \mathbf{S}\rangle$  is given by expression

$$\langle\mathbf{L} \cdot \mathbf{S}\rangle = \frac{1}{2}[J(J+1) - L(L+1) - S(S+1)]. \quad (26)$$

The corresponding radial part of the wave function for a given orbital angular momentum  $L$  is a solution of the Schrödinger equation

$$\left(-\frac{\hbar^2}{m_Q}\nabla^2 + V_{Q\bar{Q}}(r) - E\right)\psi_{LL_3}(\mathbf{r}) = 0, \quad (27)$$

where an angular part of the wave function  $\psi_{LL_3}(\mathbf{r})$  is represented in terms of the spherical harmonics  $Y_{LL_3}(\hat{\mathbf{r}})$ .

In order to solve Eq. (27) numerically, we will follow the Gaussian expansion method (see review [49]). Firstly, we expand the state vector  $|\psi_{LL_3}\rangle$  in terms of a set of basis vectors  $\{|\phi_{nLL_3}\rangle; n = 1, 2, \dots, n_{\max}\}$  as

$$|\psi_{LL_3}\rangle = \sum_{n=1}^{n_{\max}} C_n^{(L)} |\phi_{nLL_3}\rangle. \quad (28)$$

Secondly, we express the basis wave functions in the spherical coordinates

$$\phi_{nLL_3}(\mathbf{r}) = \phi_{nL}^G(r) Y_{LL_3}(\hat{\mathbf{r}}). \quad (29)$$

The radial part of wave function is expressed in terms of the Gauss functions

$$\phi_{nL}^G(r) = \left(\frac{2^{2L+7/2} r_n^{-2L-3}}{\sqrt{\pi}(2L+1)!!}\right)^{1/2} r^L e^{-(r/r_n)^2}, \quad (30)$$

where  $r_n$  are variational parameters. One should note that the set of the wave functions  $\{\phi_{nLL_3}(\mathbf{r}); n = 1, 2, \dots, n_{\max}\}$  are properly normalized while they do not need to satisfy the orthogonality condition, i.e. they consist of a non-orthogonal basis. To obtain high accuracy by using the expansion in Eq. (28) one should optimize the set of variational parameters  $\{r_n; n = 1, 2, \dots, n_{\max}\}$ . We follow an optimization discussed in Ref. [49] and express the variational parameters by using a geometric progression

$$r_n = r_1 a^{n-1}, \quad n = 1, 2, \dots, n_{\max}. \quad (31)$$

Thus, the number of variational parameters is reduced down to three, i.e.  $\{r_1, a, n_{\max}\}$  or  $\{r_1, r_{\max}, n_{\max}\}$ .

The expansion coefficients  $C_n^{(L)}$  in Eq. (28) and the eigenenergy  $E$  are determined by employing the Rayleigh-Ritz variational principle. This leads to a gen-

eralized matrix eigenvalue problem

$$\sum_{n=1}^{n_{\max}} \left( K_{mn}^{(L)} + V_{mn}^{(L)} - E N_{mn}^{(L)} \right) C_n^{(L)} = 0, \quad (32)$$

$$m = 1, 2, \dots, n_{\max},$$

where the matrix elements of the corresponding kinetic and potential energies are obtained by

$$T_{mn}^{(L)} = \langle \phi_{mLL_3} | \frac{\hat{p}^2}{m_Q} | \phi_{nLL_3} \rangle = \frac{\hbar^2(2L+1)}{m_Q(r_m^2 + r_n^2)} N_{mn}^{(L)}, \quad (33)$$

$$V_{mn}^{(L)} = \langle \phi_{mLL_3} | V_{Q\bar{Q}}(r) | \phi_{nLL_3} \rangle = \frac{2^{2L+7/2}}{\sqrt{\pi}(2L+1)!! (r_m r_n)^{L+3/2}} \int_0^\infty r^{2(L+1)} \exp \left\{ -\frac{r^2(r_m^2 + r_n^2)}{r_m^2 r_n^2} \right\} V_{Q\bar{Q}}(r) dr, \quad (34)$$

$$N_{mn}^{(L)} = \langle \phi_{mLL_3} | \phi_{nLL_3} \rangle = \left( \frac{2r_m r_n}{r_m^2 + r_n^2} \right)^{L+3/2}. \quad (35)$$

Because of Eq. (31), the overlap matrix element between the nearest neighborhoods

$$N_{n+1,n}^{(L)} = \left( \frac{2}{1+a^2} \right)^{L+3/2} \quad (36)$$

is a constant that is independent of  $n$ . This is one of the reasons why the expansion works very well. In a practical calculation  $a > 1$  and for the farthest neighborhoods ( $|n-m| = k \gg 1$ ) an orthogonality is approximately satisfied, i.e. the corresponding overlap matrix element becomes small,  $N_{mn}^{(L)} \sim 2a^{-k-2}$ .

#### IV. RESULTS AND DISCUSSIONS

In the present work, we set up three different models, depending on how to fix the numerical values of the relevant parameters. The first model is merely a nonrelativistic potential model based only on the Coulomb-like potential and the linear scalar one [44] without any contributions from the instanton vacuum. We will call it model without instantons (MWOI) and list the corresponding set of parameters in Table I. We do not intend

TABLE I. Parameters corresponding to each model. MWOI represents the model without any instanton contributions, whereas M-I and M-IIb contain them as explained in Ref. [34].

The model	$\rho$ [fm]	$R$ [fm]	$\Delta m_I$ [GeV]	$\alpha_s$ [GeV]	$\kappa$ [GeV <sup>2</sup> ]	$\sigma$ [GeV]
MWOI	-	-	-	0.2068	0.1746	5.0248
M-I	0.33	1.00	0.0676	0.3447	0.1520	0.9331
M-IIb	0.36	0.89	0.1357	0.4588	0.1279	0.5650

to carry out any fine tuning to the experimental data but

we concentrate on nonperturbative physics as to how the instanton-induced potentials have an effect on the charmonium spectrum. We also discuss physical implications of the parameters involved in the present model, including both the instanton parameters and other ones such as  $m_Q$ ,  $\kappa$  and  $\alpha_s$ . For example, while the charm-quark mass  $m_c$  is often treated as a free parameter, we will not consider it as a free parameter. Once the instanton effects are taken in to account,  $m_c$  appears as a sum of the current quark mass  $m_c^{\text{current}} = 1.275 \text{ GeV}$  and the dynamical contribution to the mass arising from the instanton vacuum,  $\Delta m_I$ , i.e.  $m_Q = m_c^{\text{current}} + \Delta m_I$  (see detailed discussions in Refs. [34, 35, 53]). The remaining three parameters  $\alpha_s$ ,  $\kappa$  and  $\sigma$  will be fitted to experimentally known masses of six charmonia that are taken from the  $S$ -wave ones. By doing that, we fix the parameters appearing in the central part of the potentials, while those of the spin-dependent parts are automatically determined. Note again that the charm-quark mass is not a free parameter. So, the spin-orbit and tensor potentials must come out naturally as in Eq. (5) and Eq. (20). We list the numerical values of all the parameters corresponding to each model in Table I, which were fixed as explained above.

In Table II, we present the results of each model in comparison with the experimental data [50] listed in the last column. The masses of the six  $S$ -wave charmonia are used as input, as noted in the second column. As shown from the results of the MWOI listed in the third column of Table II, the results on the masses of the  $S$ -wave charmonia are somewhat deviated from the experimental data. If one had released the charm-quark mass to be a mere free parameter, we would have described the experimental data very well. For example, various potential models adopt larger values of  $m_c$  than in the present work, since they yield better results, compared

TABLE II. Results on the masses of the  $c\bar{c}$  states, given in unit of MeV. The second column denotes explicitly those of the  $S$ -wave charmonia used as input to fix the parameters ( $\alpha_s$ ,  $\kappa$  and  $\sigma$ ) for each model. The third column lists the results from the original potential without the instanton-induced potentials, where as the fourth and fifth column show those from Model I and Model IIb, respectively.

State	Input	MWOI	M-I	M-IIb	Exp. [50]
$J/\psi(1^3S_1)$	3097	3084	3094	3096	$3096.900 \pm 0.006$
$\eta_c(1^1S_0)$	2983	3027	2998	2983	$2983.9 \pm 0.5$
$\psi(2^3S_1)$	3686	3635	3656	3675	$3686.097 \pm 0.025$
$\eta_c(2^1S_0)$	3640	3590	3615	3638	$3637.6 \pm 1.2$
$\psi(3^3S_1)$	4040	4067	4069	4071	$4039 \pm 1$
$\eta_c(3^1S_0)$		4026	4041	4047	
$\psi(4^3S_1)$	4415	4443	4422	4398	$4421 \pm 4$
$\eta_c(4^1S_0)$		4405	4400	4379	
$\chi_{c2}(1^3P_2)$		3428	3607	3740	$3556.17 \pm 0.07$
$\chi_{c1}(1^3P_1)$		3437	3589	3715	$3510.67 \pm 0.05$
$\chi_{c0}(1^3P_0)$		3415	3551	3673	$3414.71 \pm 0.30$
$h_c(1^1P_1)$		3430	3599	3727	$3525.38 \pm 0.11$
$\chi_{c2}(2^3P_2)$		3888	4039	4138	$3927.2 \pm 2.6$
$\chi_{c1}(2^3P_1)$		3890	4030	4125	
$\chi_{c0}(2^3P_0)$		3866	4006	4098	$3862^{+26+40}_{-32-13}$
$h_c(2^1P_1)$		3887	4039	4134	
$\chi_{c2}(3^3P_2)$		4281	4414	4466	
$\chi_{c1}(3^3P_1)$		4280	4394	4455	
$\chi_{c0}(3^3P_0)$		4256	4375	4436	
$h_c(3^1P_1)$		4278	4402	4463	
$\psi_3(1^3D_3)$		3692	3830	3929	
$\psi_2(1^3D_2)$		3718	3836	3927	$3822.2 \pm 1.2$
$\psi(1^3D_1)$		3730	3830	3914	$3778.1 \pm 1.2$
$\eta_{c2}(1^1D_2)$		3708	3837	3930	
$\psi_3(2^3D_3)$		4104	4238	4311	
$\psi_2(2^3D_2)$		4124	4242	4310	
$\psi(2^3D_1)$		4131	4241	4303	$4191 \pm 5$
$\eta_{c2}(2^1D_2)$		4116	4245	4314	

to the experimental data. However, such a fitting procedure would obscure the physical meaning of the quark mass  $m_Q$ . We want to emphasize that the heavy-quark mass itself is a physical and dynamical quantity that can be also influenced by both perturbative and nonperturbative interactions. Thus, one needs to analyze carefully the effects of the charm-quark mass on a relevant physical system. In fact, the quarkonia provides a system appropriate for scrutinizing the physical implications of the charm-quark mass. In particular, the effects from the instanton vacuum put us on the right track. Using  $m_c$  with the instanton contribution added, we are able to fit better the three parameters to the masses of the six  $S$ -wave charmonia.

In the instanton liquid model of the QCD vacuum, one can estimate the instanton contribution to the current quark mass. In the light-quark systems, the generation of the mass is fully dynamical, so that almost all the constituent quark mass originates from the sponta-

neous breaking of chiral symmetry. When it comes to the heavy-quark systems, one needs also to consider them, though the nonperturbative effects are not as much significant as in the case of the light hadrons. In Table I, the explicit values of  $\Delta m_I$  due to the instanton effects are presented for each model. The strength of the instanton effects depends on the instanton density  $n \sim (\rho/R)^4$  and the acquired mass  $\Delta m_I$  is proportional to it (compare the value in M-I with that in M-IIb, listed in Table I).

The results of calculations presented in Table II show that M-I describes the mass spectrum of the charmonia quite well even up to the  $D$ -wave charmonia. In particular, the mass of the  $D$ -wave charmonium  $\psi_2(1^3D_2)$  is much improved by the instanton effects in M-I. On the other hand and although it gives better fit to  $S$ -wave states, M-IIb does not show any improvement in comparison with the MWOI as related to  $\psi_2(1^3D_2)$ . It indicates that the original values of the instanton parameters  $\rho$  and  $R$  yield the better results, which are in fact expected. Those values employed in M-IIb were determined when the  $1/N_c$  meson-loop corrections are involved, which is not the case of the present work.

Another important issue lies in the running strong coupling constant  $\alpha_s$ . Since the Coulomb-like potential arises from OGE in pQCD, the value of  $\alpha_s(\mu)$  should be taken from pQCD at a proper scale related to the charmonia. In fact, the static Coulomb potential was extensively studied within the framework of pQCD, higher-order corrections being even taken into account [28–32]. However, a fitted value of  $\alpha_s$  was used in many models because it is simpler and phenomenologically more favorable than that from pQCD. At the one-loop level it is given by expression

$$\alpha_s(\mu) = \frac{4\pi}{\beta_0} \frac{1}{\ln(\mu^2/\Lambda_{\text{QCD}}^2)}, \quad (37)$$

where the  $\beta$  function at the one-loop level is equal to be  $\beta_0 = (11N_c - 2N_f)/3$ . The dimensionful parameter of QCD is given as  $\Lambda_{\text{QCD}} = 0.217 \text{ GeV}$  [50] and  $\mu$  stands for a specific scale at which the value of  $\alpha_s$  is evaluated. It is usual to take  $\mu \approx m_c$  for the charmonia.

The value of  $\alpha_s$  at the one-loop level can be easily computed by using Eq. (37), once a proper scale  $\mu$  is given. Considering the fact that MWOI, M-I and M-IIb have different charm-quark masses, we can calculate the value of  $\alpha_s$  corresponding to a specific model by using the charm-quark mass of the model as its intrinsic scale. The results for M-I and M-IIb are obtained respectively as  $\alpha_s(\mu = 1.343 \text{ GeV}) = 0.4137$  and  $\alpha_s(\mu = 1.411 \text{ GeV}) = 0.4029$ , which are slightly larger or smaller than the corresponding fitted values listed in Table I, respectively. On the other hand, the value of  $\alpha_s$  for MWOI turns out to be  $\alpha_s(\mu = 1.275 \text{ GeV}) = 0.4258$ , which is approximately two times larger than the fitted value 0.2068. This comparison already demonstrates that in the presence of the instanton-induced interaction one is allowed to use a more *physical* strong coupling constant

for the Coulomb-like potential, based firmly on perturbative QCD.

The origin of the confining scalar potential is not much known theoretically and the string tension  $\kappa$  is considered as a phenomenological parameter, though it can be related to Regge trajectories within some models [54]. The parameter  $\kappa$  was often determined by the charmonium spectrum together with the *effective* strong coupling constant [23, 52, 54] and the numerical value of  $\kappa$  is known approximately to be  $\kappa \approx 0.18 \text{ GeV}^2$  (see a review [54]). In the present work, we fix it to be  $0.175 \text{ GeV}^2$  for the MWOI, which is very close to the above-given value. However, once we introduce the instanton-induced potential, we have to use smaller values of  $\kappa$ , because the central part of instanton-induced potential has almost a linearly rising behavior and then is saturated as the inter-distance of the quarks increases [34, 35]. It means that the instanton effects reduce the strength of the linear scalar potential. In other words, the instanton-induced interactions contribute partially to the confining potential in a general form

$$V_{\text{conf}}(r) = \text{const.} + \kappa r + \text{possible nonlinear terms.} \quad (38)$$

For example, the leading order contribution from instantons in Eq.(8) to the total  $Q\bar{Q}$  potential at small distances can be treated as a nonlinear corrections to the linearly raising potential. In this context, the instanton induced potential at large distances  $(4\pi\rho^3/N_c R^4)\mathcal{I}_0$  has a meaning of partial contribution to the constant part of confining potential in Eq. (38).

Finally, we discuss the smearing parameter  $\sigma$  that was introduced to avoid the singular behavior of the point-like spin-spin interactions. Its value gets smaller if the instanton-induced potentials are included. Note that the point-like interaction is actually an artifact of an  $\mathcal{O}(v_q^2/c^2)$  expansion of the  $T$ -matrix [51]. Introducing the instanton-induced potential<sup>1</sup>, one can partially solve the divergence problem that arises from the singular spin-spin interactions.

## V. SUMMARY AND OUTLOOK

In the present work, we aimed at investigating the instanton effects on the charmonium mass spectrum, based on a nonrelativistic potential model. Though we fixed the relevant parameters by using the masses of the six

$S$ -wave charmonia, we did not intend to carry out the fine-tuning of the parameters. The results showed that the instanton-induced potentials improved the mass spectrum with the original values of the average size of the instanton and the average inter-distance between instantons. We discussed also the physical implications of the parameters such as the charm-quark mass, the running strong coupling constant, the string tension, and the smearing factor. The instanton-induced potentials enable one to understand more clearly these physical parameters.

Though we considered certain nonperturbative contributions to the mass spectrum of the charmonia from the instanton vacuum, we still need to take into account yet additional effects from the instantons. Recently, it was shown that the instanton effects or the screening effects in the Coulomb-like potential of one-gluon exchange will appear due to gluon propagation in instanton media [55]. Since the gluon is screened by the instanton effects and as a result it acquires an effective mass, we have in addition a Yukawa-type potential between the heavy quark and heavy anti-quark. One needs to examine how this screened potential may influence the charmonium masses.

Another interesting issue is related to strong decays of excited charmonia, which involve the pions. Since the pion is the pseudo-Goldstone boson that appears from the spontaneous breakdown of chiral symmetry, the instanton effects will come into critical play in describing these decay processes. Related works are under way.

## ACKNOWLEDGMENTS

We are grateful to P. Gubler, A. Hosaka, T. Maruyama, M. Oka and M. Musakhanov for useful discussions. H.-Ch.K wants to express his gratitude to the members of the Advanced Science Research Center (ASRC) at Japan Atomic Energy Agency (JAEA) for the hospitality, where part of the present work was done. This work is supported by the Basic Science Research Program through the National Research Foundation (NRF) of Korea funded by the Korean government (Ministry of Education, Science and Technology, MEST), Grant Numbers 2016R1D1A1B03935053 (UY) and NRF2018R1A2B2001752 (HChK). The work was also partly supported by RIKEN iTHES Project.

---

<sup>1</sup> Note that the spin-dependent parts of the instanton-induced potentials are regular.

- 
- [1] S. K. Choi *et al.* [Belle Collaboration], Phys. Rev. Lett. **91** (2003) 262001.
  - [2] B. Aubert *et al.* [BaBar Collaboration], Phys. Rev. D **71** (2005) 071103.
  - [3] B. Aubert *et al.* [BaBar Collaboration], Phys. Rev. Lett. **95** (2005) 142001.

- [4] K. Abe *et al.* [Belle Collaboration], Phys. Rev. Lett. **98** (2007) 082001.
- [5] S. K. Choi *et al.* [Belle Collaboration], Phys. Rev. Lett. **100** (2008) 142001.
- [6] A. Bondar *et al.* [Belle Collaboration], Phys. Rev. Lett. **108** (2012) 122001.
- [7] Z. Q. Liu *et al.* [Belle Collaboration], Phys. Rev. Lett. **110** (2013) 252002.
- [8] M. Ablikim *et al.* [BESIII Collaboration], Phys. Rev. Lett. **110** (2013) 252001.
- [9] M. Ablikim *et al.* [BESIII Collaboration], Phys. Rev. Lett. **111** (2013) 242001.
- [10] R. Aaij *et al.* [LHCb Collaboration], Phys. Rev. Lett. **110** (2013) 222001.
- [11] M. Ablikim *et al.* [BESIII Collaboration], Phys. Rev. Lett. **112** (2014) 022001.
- [12] R. Aaij *et al.* [LHCb Collaboration], Phys. Rev. Lett. **112** (2014) 222002.
- [13] R. Aaij *et al.* [LHCb Collaboration], Phys. Rev. D **92** (2015) 112009.
- [14] C. Z. Yuan [BESIII Collaboration], Front. Phys. China **10** (2015) 101401.
- [15] C. Z. Yuan [Belle Collaboration], arXiv:1512.03281 [hep-ex].
- [16] E. S. Swanson, Phys. Rept. **429** (2006) 243.
- [17] E. Eichten, S. Godfrey, H. Mahlke and J. L. Rosner, Rev. Mod. Phys. **80** (2008) 1161.
- [18] M. B. Voloshin, Prog. Part. Nucl. Phys. **61** (2008) 455.
- [19] N. Brambilla *et al.*, Eur. Phys. J. C **71** (2011) 1534.
- [20] S. L. Olsen, Front. Phys. **10** (2015) 101401.
- [21] H. X. Chen, W. Chen, X. Liu, Y. R. Liu and S. L. Zhu, Rept. Prog. Phys. **80** (2017) 076201.
- [22] E. Eichten, K. Gottfried, T. Kinoshita, J. B. Kogut, K. D. Lane and T. M. Yan, Phys. Rev. Lett. **34** (1975) 369 [Phys. Rev. Lett. **36** (1976) 1276].
- [23] E. Eichten, K. Gottfried, T. Kinoshita, K. D. Lane and T. M. Yan, Phys. Rev. D **17** (1978) 3090 [Phys. Rev. D **21** (1980) 313].
- [24] L. Susskind, "Coarse Grained Quantum Chromodynamics," in Weak and Electromagnetic Interactions at high energies: Proceedings. Edited by Roger Balian and Christopher H. Llewellyn Smith (N.Y., North-Holland, 1977).
- [25] T. Appelquist, M. Dine and I. J. Muzinich, Phys. Lett. B **69** (1977) 231.
- [26] T. Appelquist, M. Dine and I. J. Muzinich, Phys. Rev. D **17** (1978) 2074.
- [27] W. Fischler, Nucl. Phys. B **129** (1977) 157.
- [28] M. Peter, Phys. Rev. Lett. **78** (1997) 602.
- [29] M. Peter, Nucl. Phys. B **501** (1997) 471.
- [30] Y. Schroder, Phys. Lett. B **447** (1999) 321.
- [31] A. V. Smirnov, V. A. Smirnov and M. Steinhauser, Phys. Rev. Lett. **104** (2010) 112002.
- [32] C. Anzai, Y. Kiyo and Y. Sumino, Phys. Rev. Lett. **104** (2010) 112003.
- [33] K. G. Wilson, Phys. Rev. D **10** (1974) 2445.
- [34] U. T. Yakhshiev, H.-Ch. Kim, M. M. Musakhanov, E. Hiyama and B. Turimov, Chin. Phys. C **41** (2017) 083102.
- [35] D. Diakonov, V. Y. Petrov and P. V. Pobylitsa, Phys. Lett. B **226** (1989) 372.
- [36] D. Diakonov and V. Y. Petrov, Nucl. Phys. B **245** (1984) 259.
- [37] D. Diakonov and V. Y. Petrov, Nucl. Phys. B **272** (1986) 457.
- [38] D. Diakonov, Prog. Part. Nucl. Phys. **51** (2003) 173.
- [39] E. Eichten and F. Feinberg, Phys. Rev. D **23** (1981) 2724.
- [40] E. V. Shuryak, Nucl. Phys. B **203** (1982) 93.
- [41] H.-Ch. Kim, M. M. Musakhanov and M. Siddikov, Phys. Lett. B **633** (2006) 701.
- [42] K. Goeke, M. M. Musakhanov and M. Siddikov, Phys. Rev. D **76** (2007) 076007.
- [43] K. Goeke, H.-Ch. Kim, M. M. Musakhanov and M. Siddikov, Phys. Rev. D **76** (2007) 116007.
- [44] T. Barnes, S. Godfrey and E. S. Swanson, Phys. Rev. D **72**, 054026 (2005).
- [45] M. C. Chu, J. M. Grandy, S. Huang and J. W. Negele, Phys. Rev. D **49** (1994) 6039.
- [46] J. W. Negele, Nucl. Phys. Proc. Suppl. **73** (1999) 92.
- [47] T. A. DeGrand, Phys. Rev. D **64** (2001) 094508.
- [48] P. Faccioli and T. A. DeGrand, Phys. Rev. Lett. **91** (2003) 182001.
- [49] E. Hiyama, Y. Kino and M. Kamimura, Prog. Part. Nucl. Phys. **51** (2003) 223.
- [50] M. Tanabashi *et al.* (Particle Data Group), Phys. Rev. D **98**, 030001 (2018).
- [51] T. Barnes and G. I. Ghandour, Phys. Lett. **118B** (1982) 411.
- [52] C. Quigg and J. L. Rosner, Phys. Rept. **56** (1979) 167.
- [53] S. Chernyshev, M. A. Nowak and I. Zahed, Phys. Lett. B **350** (1995) 238 [hep-ph/9409207].
- [54] G. S. Bali, Phys. Rept. **343** (2001) 1 [hep-ph/0001312].
- [55] M. Musakhanov and O. Egamberdiev, Phys. Lett. B **779** (2018) 206 [arXiv:1706.06270 [hep-ph]].